CHAPTER 3

Elastic Modulus and Tensile Behaviour

3.1 INTRODUCTION

This chapter presents the effect of different heat treatments on elastic modulus and tensile properties of the alloy Ti-13Nb-13Zr. This alloy was subjected to solution treatment at two different temperatures and quenched at different temperatures. Influence of heat treatment was investigated on the microstructure, microhardness, elastic modulus, and tensile strength. The alloy was given three different heat treatments, as shown in Figure 3.1. Two samples were solution treated at 900°C (above β transus~735°C) for 1 hour; one was quenched in water at room temperature (25°C) and the other in alcohol maintained at sub-zero temperature (–30°C), and these are designated as 900WQ and 900SZQ, respectively. Another sample was solution treated at 660°C (below β transus) for 1 h and quenched in water at room temperature (25°C) and was designated as 660WQ.

Figure 3.1 Heat treatment outline for the alloy Ti-13Nb-13Zr.

3.2 MICROSTRUCTURAL CHARACTERIZATION

The optical microstructures in the as-received (AR) and different heat-treated conditions are shown in Figure 3.2. The various phases identified in the different heat-

treated conditions may be seen from the XRD peaks (Figure 3.3). The microstructures of all the samples showed variants of alpha (α) phase within beta (β) phase matrix. XRD revealed primary α and β phases in the AR condition (Figure 3.2a). The 660WQ (Figure 3.2b) condition showed presence of α′′(orthorhombic) martensite along with α and β phases. It may be seen that, in general, the transformed α platelets are much finer in the AR condition than in the 660WQ.

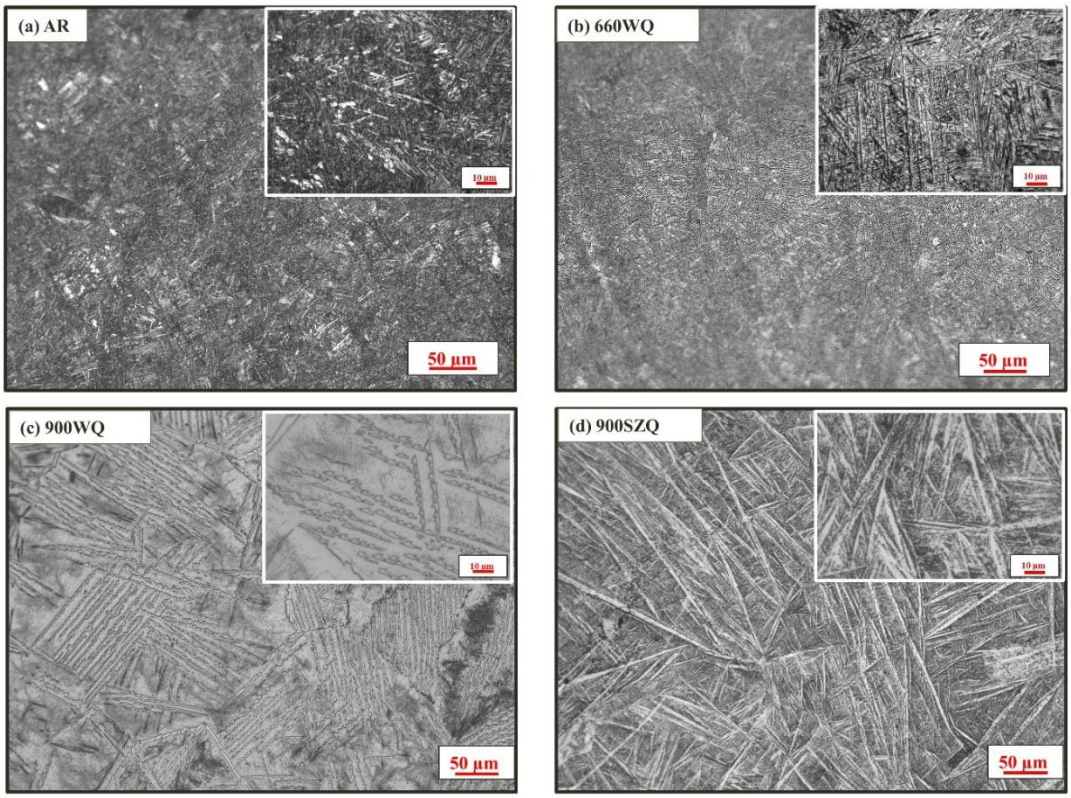

Figure 3.2 Optical microstructures of the Ti-13Nb-13Zr alloy in different conditions (a) AR, (b) 660WQ, (c) 900WQ and (d) 900SZQ. Magnified views are shown in the insets.

It may be seen that the microstructures in the 900WQ (Figure 3.2c) and 900SZQ (Figure 3.2d) conditions are much coarser than 660WQ (Figure 3.2b). The β solution treated and sub-zero quenched samples contain α′′, in addition to α′ and β phases, as observed in the water quenched condition. It is interesting to note that orthorhombic α′′ was also formed in the 900SZQ condition.

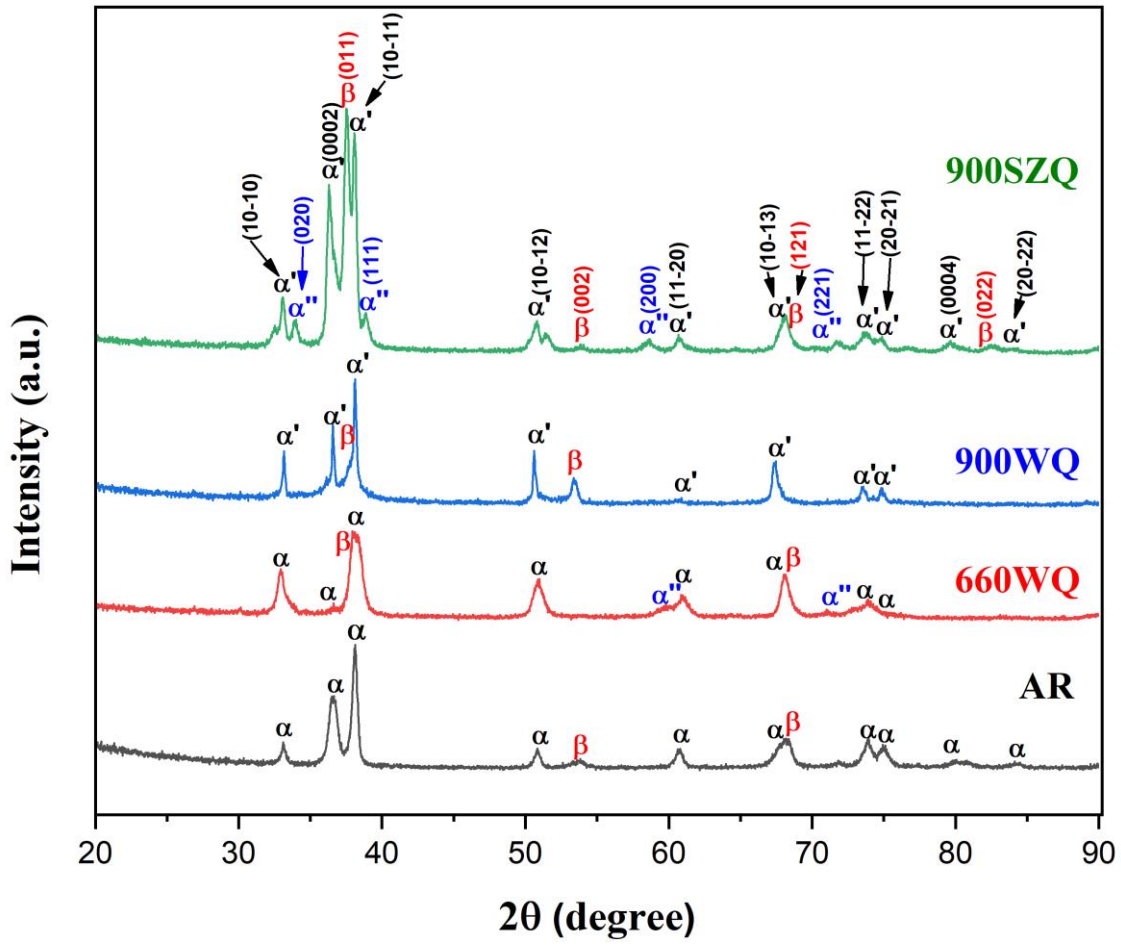

Figure 3.3 XRD patterns of the Ti-13Nb-13Zr alloy in different conditions.

Figure 3.3 displays XRD patterns of the Ti-13Nb-13Zr alloy in different heat-treatment conditions. In order to calculate the volume fraction of constituent phases, the integrated areas of all the diffraction peaks from XRD were fitted using Pseudo-Voigt function in the software X-pert Highscore [205–207]. The volume fraction of primary α in the AR and 660WQ conditions was estimated by using the equation given below:

$$V_\alpha = \frac{A_\alpha}{A_\alpha + A_\beta} \qquad \text{(Equation 3.1)}$$

Also, the volume fraction of α′ and α′′ martensite in the 900WQ and 900SZQ conditions was estimated from a similar equation:

$$V_{\alpha'} = \frac{A_{\alpha'}}{A_{\alpha''}+A_{\alpha'}+A_{\beta}} \quad \text{(Equation 3.2)}$$

where A_{α}, A_{β}, $A_{\alpha'}$, and $A_{\alpha''}$ are the total integrated areas under the peaks of the α, β, α′, and α′′ phases, respectively, calculated after fitting the curves with the help of a software X-pert High Score Plus. The volume fraction of different phases was estimated from the XRD patterns as well as from the microstructures of the different heat-treated conditions and represented as Vol% of phases in Table 3.1.

Table 3.1 Different phases and their volume fractions in different conditions.

SR No.	**Conditions**	**Phase Constituents**	**Vol% of phases from XRD**	**Vol% of α/α′ phases from Microstructure**
1.	AR (As-received)	α+β	α(hcp)=66%, β(bcc)=34%	α(hcp)=64%
2.	660WQ (Solution treated for 1 h at 660°C and quenched in water)	α+α′′+β	α(hcp)=53%, α′′(orthorhombic)=27%, β(bcc)=20%	α(hcp)=53%
3.	900WQ (Solution treated for 1 h at 900°C and quenched in water)	α′+β	α′(hcp)=63%, β(bcc)=37%	α′(hcp)=63%
4.	900SZQ (Solution treated for 1 h at 900°C and quenched at sub-zero temperature)	α′′+α′+β	α′′(orthorhombic)=51%, α′(hcp)=37%, β(bcc)=12%	α′(hcp)=33%

The volume percentage of α′ martensite was observed to be highest (~63%) in the 900WQ condition, while α′′ martensite was found highest (~51%) in the 900SZQ condition. β phase can be seen in all the three heat-treated conditions. The volume

percentage of phases determined from XRD data and microstructures were found comparable.

3.3 MICROHARDNESS

Vickers microhardness of the different heat-treated specimens is depicted in Figure 3.4. There was variation in microhardness with respect to the rate of cooling. Microhardness was found to be maximum in the AR condition (H_V: 289±7), followed by that in 660WQ (H_V: 266±8), 900SZQ (H_V: 258±5), and 900WQ (H_V: 247±7).

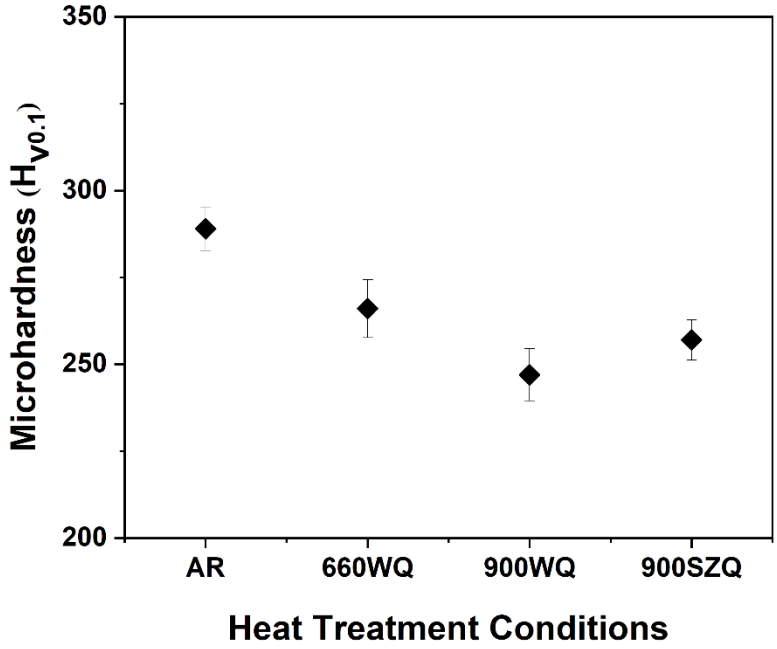

Figure 3.4 Variation of microhardness in different conditions.

3.4 ELASTIC MODULUS

Figure 3.5 represents elastic modulus (E) data obtained from the ultrasonic velocity gauge technique for the different heat-treated samples. It may be seen that the elastic modulus decreases with increase in the cooling rate. The modulus of elasticity of all the heat-treated samples varies from 84 GPa to 59 GPa. The samples solution treated,

below the β transus temperature, exhibited modulus higher than the samples solution treated above β transus.

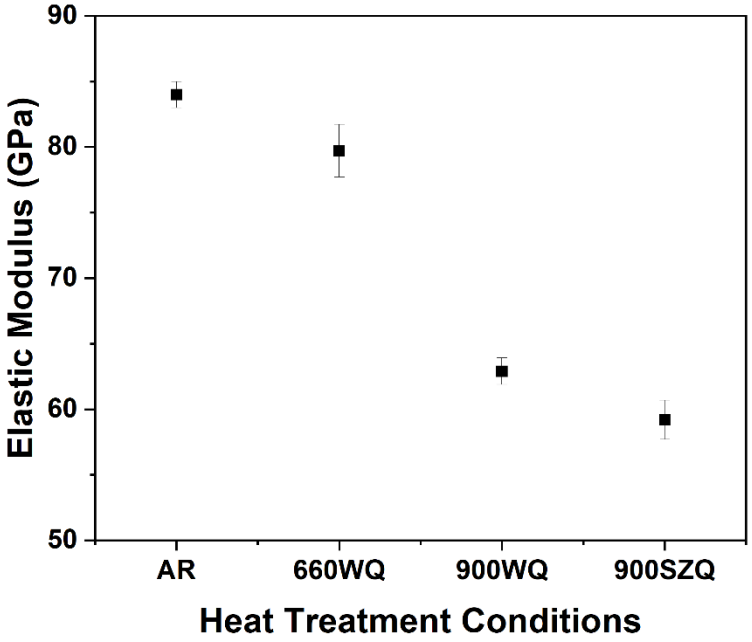

Figure 3.5 Elastic modulus of Ti-13Nb-13Zr alloy in different conditions, measured by ultrasonic testing.

However, there is not much change in elastic modulus of water quenched and sub-zero quenched samples. A large decrease in the modulus (E: 59±0.5 GPa) was observed for the specimen quenched from the β phase field for the 900SZQ condition.

3.5 TENSILE PROPERTIES

The tensile properties measured from tensile tests of the different heat-treated samples, such as elastic modulus (E), yield strength (YS), ultimate tensile strength (UTS), elongation (TE), and reduction in area (RA), are presented in Table 3.2 and schematically shown by typical stress-strain curves in Figure 3.6. Elastic moduli values obtained from the tensile tests and ultrasonic testing were found to be comparable. Yield strength of the AR sample was found to be highest among all the samples. The 660WQ showed

moderate yield strength among all the tested samples. However, there is no significant variation in yield strength of the 900WQ and 900SZQ samples.

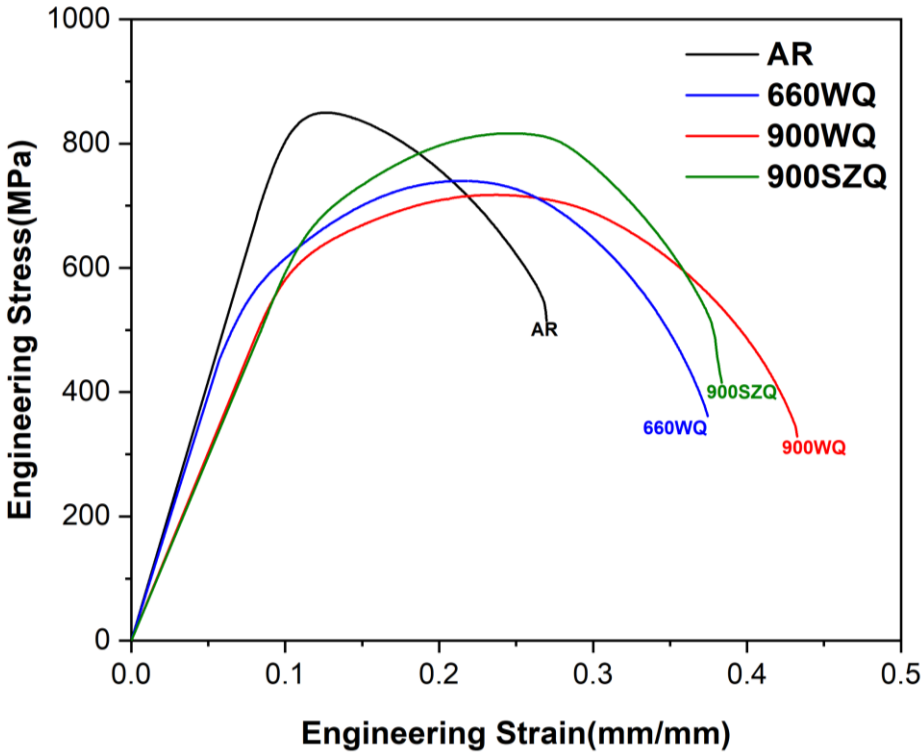

Figure 3.6 Typical stress-strain curves of Ti-13Nb-13Zr alloy in different conditions.

Table 3.2 Tensile properties* in the as-received and different heat-treated conditions.

Sr. No.	Condition	TENSILE TEST					Ultrasonic Technique
		E (GPa)	YS (MPa)	UTS (MPa)	TE (%)	RA (%)	E (GPa)
1.	AR	83.7±0.6	791±24	849±20	21±1.9	49.65±2	84.06±0.2
2.	660WQ	79.0±0.8	610±22	763±35	33±0.8	64.68±3	79.72±0.4
3.	900WQ	60.6±0.8	578±25	717±24	37±1.2	69.33±2	62.90±0.3
4.	900SZQ	59.2±0.5	564±23	775±44	32±1.5	64.50±4	58.62±0.2

*****Elastic Modulus (E), Yield Strength (YS), Ultimate Tensile Strength (UTS), Total Elongation (TE) and Reduction in Area (RA)

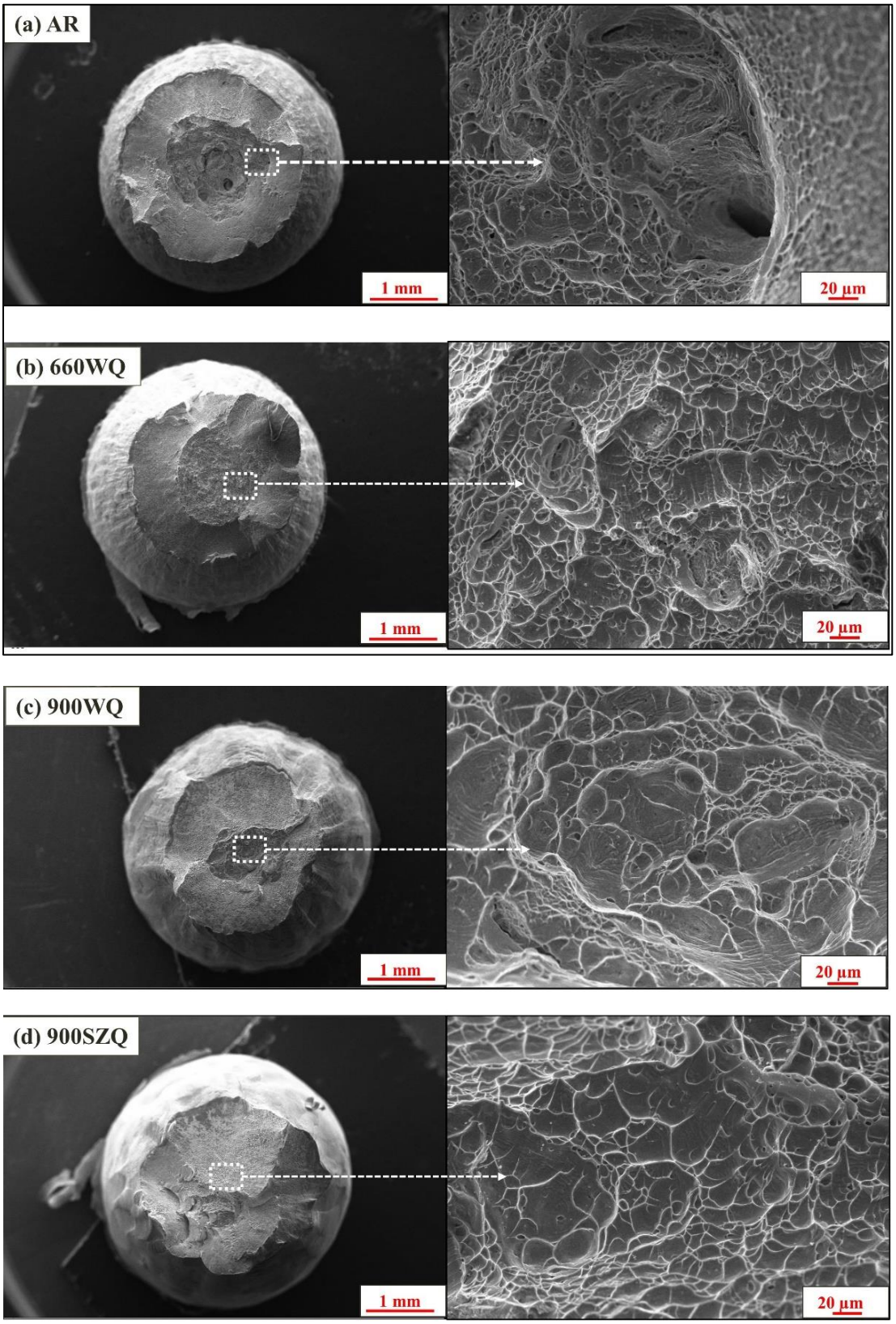

Figure 3.7 SEM fractographs of tensile tested samples with different conditions: (a) AR, (b) 660WQ, (c) 900WQ and (d) 900SZQ, showing dimple morphology.

The 900WQ and 900SZQ samples showed increase in ductility. In case of AR sample, yield strength is higher but ductility is lower. The samples solution treated in the β phase field and quenched at sub-zero showed slightly lower ductility as compared to the other water quenched samples. The SEM images at low magnification in Figure 3.7 show fracture surfaces of the different samples after tensile testing. From the fractographs of Figure 3.7a, shallow and fine dimples are seen clearly in the images at right hand side, at higher magnification.

Dimple morphology throughout the fracture surface of samples shows ductile fracture. The AR samples showed mean dimple size of 9.89±2.5 μm along with some microvoids indicating lower ductility (Figure 3.7a). The mean dimple size measured from Figure 3.7 (b to d) was 18.65±4.5 μm, 20.7±7 μm and 17.9 ±5.6 μm for the 660WQ, 900WQ and 900SZQ samples, respectively. The ductility parameters, total elongation and reduction in area shown in Table 3.2 can be related with the size of dimples on the fracture surface.

3.6 DISCUSSION

The microstructure of the as-received material showed basket-weave type Widmanstätten α platelets in line with the earlier observation of Krishnan et al. [208]. The AR condition (Figure 3.2a) represents the type of microstructure resulting from β-solution treatment and cooling in air, in which a part of the prior β phase gets transformed into fine 'basket-weave' type α platelets [96]. The α platelet size depends on the cooling rate. The fine α platelets in Figure 3.2a in the AR condition, are similar to those observed in the earlier observations [96,209]. The fine α platelets present in the AR sample act as crack nucleation sites and reduce the ductility [39].

The primary α phase is already present in the samples solution treated at 660°C and quenched in water (660WQ) (Figure 3.2b). According to Geetha et al. [28] presence of α′′ martensite is expected in the 660WQ , α+β solution treated condition. Quenching of sample from the α+β phase-field temperature causes Nb enrichment in the β phase, owing to partitioning effect of the alloying elements and transformation to orthorhombic martensite [210]. There is sandwiching of primary α phase within transformed β, which increased the local plastic strain and caused strengthening and rise in microhardness [96]. There is slight coarsening of the primary α phase from solution treatment in the (α+β) phase field, which caused increase in the lath size compared to the AR condition. The presence of martensite α′′ in small amount in the 660WQ condition lowers the strength and hardness compared to the AR condition.

In general, during quenching, if the cooling rate is high enough, there is formation of martensite structure [211]. The Ti-Nb alloys can form metastable martensites depending upon the niobium content i.e. hexagonal α′ for Nb<13% and orthorhombic α′′ martensite for Nb>13% [212]. In the present alloy containing Nb~13%, α′as well as α′′ martensites were formed on sub-zero quenching from the β phase field [213].

However, there is formation of α′ in the both 900WQ and 900SZQ samples (Figure 3.2c). The martensite variants have lower hardness compared to β phase [213]. Therefore, presence of α′/α′′ phases and lack of α phase reduces the microhardness of 900WQ and 900SZQ specimens. The combination of softer α′′ and β phases in the case of the 900SZQ samples (Figure 3.2d) showed decrease in hardness and yield strength compared with that of the 660WQ sample, that consisted of mainly primary α and β with minimal amount of α′′ martensite [96].

The elastic modulus of implants of the stainless steel (~206 GPa) and Cobalt based alloys (~240 GPa) is considerably higher than that of titanium alloys (121-57 GPa). In titanium alloys, elastic modulus is mainly dependent on the microstructure [214]. The modulus determination in titanium alloys can be done by relative volume fraction of the different phases. A proper value of elastic modulus in the implant material is necessary to have good mechanical compatibility with the human cortical bone. Therefore, it is important to understand the relationship of elastic modulus with microstructure. The volume fraction of different phases depends upon the prior thermomechanical and heat treatment given to the alloy. The martensite phase α′′ causes decrement in modulus due to reorientation and detwinning effect of α′′ variants. The previous reports have shown that proper combination of β and α′′ offers lowest modulus among the other phase combinations, and the relative variation in modulus values for the phases follows the sequence as β<α′′<α′<α [77,215]. Furthermore, Kim et al. [216] showed that elastic modulus of the metastable-β was less than that of the stable β phase.

The AR sample with α and β phases shows higher elastic modulus than those of all the other heat-treated samples, due to high volume fraction of α phase. There is reduction in modulus value from solution treatment at 660°C and water quenching, due to formation of small amount of α′′ martensite along with α and transformed β phases. The 900WQ samples also show reduction in modulus due to the presence of softer α′ and β phases. The further reduction in the modulus of 900SZQ sample can be attributed to α′, α′′ and β phases present in the microstructure.

Table 3.3 Effect of the different processes and heat treatments on modulus and other tensile properties* of the alloy Ti-13Nb-13Zr, reported earlier.

Sr. No.	**Process/ Condition**	**YS (MPa)**	**UTS (MPa)**	**TE (%)**	**E (GPa)**
1.	Deformation at 800 °C+ Solution Treatment (ST)+Water Quenching (WQ) [96]	486 to 562	732 to 775	12 to 20	66
2.	Deformation at 800 °C+ ST+WQ+ageing [96]	924	1045	4	74
3.	Dynamic Globularization [217]	1010	1119	8.4	78
4.	Mill Annealing (as-received) [217]	619	716	15.7	81
5.	Solutionizing+ aging [125]	827	902	8.2	80
6.	As cast [124]	~665	~945	~15.1	~77
7.	ST (1000°C for 1 hr) +WQ→ cold worked (80%)→ ST (900°C for ½ hr)+WQ [217]	510	732	30	65
8.	WQ+Aged [93]	1030	900	15	79
9.	**Solutionized and Sub Zero Quenched** (Present Study)	**564**	**775**	**32**	**59**

*****Elastic Modulus (E), Yield Strength (YS), Ultimate Tensile Strength (UTS) and Total Elongation (TE)

A comparison of tensile properties of Ti-13Nb-13Zr alloy in the present investigation with those of earlier reports with slight variation in the thermomechanical treatments is shown in Table 3.3. Majumdar et al. [96] and Lin et al. [124] found low modulus of elasticity and attributed to the presence of α′ martensite and β phases. The reason for lowering of the elastic modulus was not discussed in detail by other researchers [124,125,217]. In the present study it was observed that the combined effect of α′′ martensite along with α′ and β phases in the microstructure of 900SZQ sample results in highest reduction in the modulus. Thus, the present investigation shows that the modulus of elasticity of the Ti-13Nb-13Zr alloy can be lowered merely by heat treatment,

without any prior mechanical deformation or cold work. In this condition, the alloy also possesses sufficient strength and ductility required for implant applications.

3.7 CONCLUSIONS

The main conclusions drawn from this chapter are given as follows:

1. The microstructures in the different heat-treated conditions consist of different combinations of α, β, α′′ and α′ phases with various morphologies. The AR samples showed α+β type microstructure. The 660WQ samples exhibited α+β type microstructure in addition to α′′ martensite. The 900WQ sample exhibited α′ and β phases. Along with the α′ and β phases, the 900SZQ sample revealed an additional α′′ phase.
2. The optimum tensile properties, along with lowest modulus, are observed for the sample solution treated at 900°C and sub-zero quenched. This decrease in elastic modulus is attributed to formation of α′′ and α′ martensite along with retained β phase from fast cooling, following β solution treatment.
3. The elastic modulus achieved in the present study is lowest among the various non-cold worked conditions of the alloy Ti-13Nb-13Zr in respect of those reported earlier.
4. The elongation in 900WQ condition was highest as well as the elastic modulus was low ~60 GPa. Therefore, due to its less stress shielding effect it has greater bio-compatibility we have selected this heat treatment for further improvement in other properties such as corrosion resistance, fatigue life and cell behaviour.